Bioorganic Chemistry 89 (2019) 102976

Contents lists available at ScienceDirect

Bioorganic Chemistry

journal homepage: www.elsevier.com/locate/bioorg

Synthesis, molecular modeling and biological evaluation of new pyrazolo[3,4-*b*]pyridine analogs as potential antimicrobial, antiquorum-sensing and anticancer agents

N.S. El-Gohary[a,*], M.T. Gabr[a,b], M.I. Shaaban[c]

[a] Department of Medicinal Chemistry, Faculty of Pharmacy, Mansoura University, Mansoura 35516, Egypt
[b] Department of Chemistry, University of Iowa, Iowa City, IA 52242, United States
[c] Department of Microbiology, Faculty of Pharmacy, Mansoura University, Mansoura 35516, Egypt

ARTICLE INFO

Keywords:
Pyrazolo[3,4-*b*]pyridines
Antimicrobial
Antiquorum-sensing
Anticancer
DNA-binding
Molecular modeling

ABSTRACT

New pyrazolo[3,4-*b*]pyridine analogs **2–9** were synthesized and subjected to antimicrobial testing toward chosen Gram-negative bacteria, Gram-positive bacteria and fungi. Compound **2** exhibited potent and extended-spectrum antimicrobial activity. Further, **6** and **9c** demonstrated remarkable and extended-spectrum antibacterial activity. Antiquorum-sensing activity of the new members was tested over *C. violaceum*, whereas **9c** demonstrated strong efficacy, while **2, 8b** and **9b** displayed moderate efficacy. *In vitro* anticancer assay toward HepG2, MCF-7 and Hela cancer cells manifested that **2** and **9c** are powerful and extended-spectrum anticancer agents. Additionally, **8a, 8b** and **9b** showed excellent activity toward the three cancer cells. *In vivo* anticancer assay over EAC in mice indicated that **2** and **9c** have the greatest activity. Moreover, cytotoxicity assay over WISH and W138 normal cells clarified that the checked analogs possess weak cytotoxicity toward the two normal cells. DNA-binding affinity was also tested, whereas **2, 3, 8b, 9b** and **9c** demonstrated great affinity. Molecular modeling studies revealed that the investigated compounds bind to DNA through intercalation similarly to doxorubicin. *In silico* studies revealed that the new members are anticipated to show excellent intestinal absorption.

1. Introduction

The effective remedy of an ever-increasing range of microbial infections is affected by antimicrobial resistance (AMR). AMR is a progressively critical threat to global public health, more and more infections are caused by microorganisms that fail to respond to conventional treatments [1,2]. Therefore, new challenges are desired to fight AMR, an auspicious approach to fight AMR is to target quorum sensing (QS). QS is important in regulation of bacterial gene expression *via* utilization of chemical signals called autoinducers [3]. QS allows bacterial populations to communicate and coordinate group behaviour causing pathogenicity, and hence bacterial drug resistance [4]. Quorum sensing inhibitors (QSIs) are agents that disrupt the QS system in bacteria, and hence they may provide the newest weapon in the remedy of drug-resistant bacterial infections [5].

On the other hand, cancer is a major health risk, and it is characterized by abnormal growth of cells which proliferate in an uncontrolled way and metastasize to nearby organs through bloodstream or lymph system [6]. An exemplary anticancer drug must be of selective cytotoxicity toward cancer cells without injuring normal ones. In the present days, cancer became a prime area of research, and scientists are engrossed in innovation of new anticancer agents with high potency and selectivity.

DNA intercalation has received growing interest in the development of anticancer agents based on the success of anthracyclines (e.g. doxorubicin) as anticancer therapeutics [7]. DNA intercalators bind firmly and reversibly to DNA, resulting in inhibition of DNA replication and cell death [8]. DNA intercalators such as doxorubicin (DOX) [9], mitoxantrone [10] and amsacrine [11] (Fig. 1) possess common pharmacophoric features, including planar aromatic moieties that can be inserted between DNA base pairs forming a complex which is stabilized by hydrophobic interactions, vander Waals forces and hydrogen bonding [12]. In addition, incorporation of positively charged or basic moieties (e.g. amino group or nitrogen of heterocyclic nitrogenous rings) into DNA intercalators might also play a pivotal role in increasing the affinity and selectivity of these agents [13]. The basic moieties can

* Corresponding author.
E-mail address: dr.nadiaelgohary@yahoo.com (N.S. El-Gohary).

https://doi.org/10.1016/j.bioorg.2019.102976
Received 19 February 2019; Received in revised form 5 May 2019; Accepted 6 May 2019
Available online 08 May 2019
0045-2068/

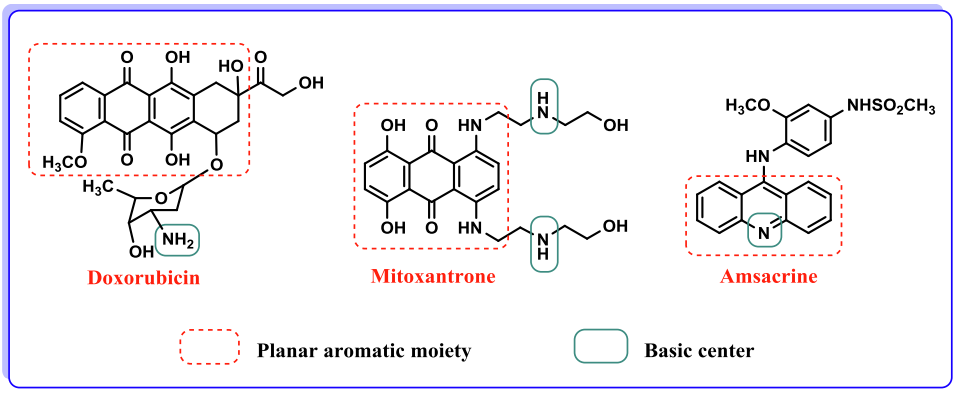

Fig. 1. Principal pharmacophoric features of DNA intercalators.

be protonated under physiological conditions and interact with negatively charged phosphate groups in DNA, resulting in more efficient binding and intercalation [14–16]. In the recent years, medicinal chemists are concerned with design and discovery of new DNA intercalators as anticancer agents [14–16].

Pyrazolo[3,4-*b*]pyridine nucleus is a prime scaffold in a variety of marketed anxiolytic-antidepressant drugs as cartazolate [17], tracazolate [18] and etazolate [19] (Fig. 2). The pyrazolo[3,4-*b*]pyridines were reported to display antibacterial [20–22], antifungal [23], antimicrobial [24–34] and anticancer [16,22,24,25,29,31–43] activities. For instance, pyrazolo[3,4-*b*]pyridines **A** [24], **B** [24], **C** [16], **D** [16], **E** [16] and **F** [25] were pronounced to show good DNA-binding affinity with promising anticancer efficacy (Fig. 3), and pyrazolo[3,4-*b*]pyridines **C** [16], **D** [16] and **E** [16] were further proved to bind to DNA through intercalation. Besides, pyrazolo[3,4-*b*]pyridines **G** [24], **H** [24], **I** [25] and **J** [25] illustrated interesting and extended-spectrum antimicrobial efficacy through targeting DNA (Fig. 4). Additionally, pyrazolo[3,4-*b*]pyridines **K** [24], **L** [24], **M** [24], **N** [25] and **O** [25] were characterized as excellent antimicrobial and anticancer agents through targeting DNA (Fig. 5). Inspired by these findings and as expansion to our previous research [24,25], new pyrazolo[3,4-*b*]pyridine candidates **2–9** with different substitutions were designed to encompass the principal pharmacophoric features of DNA intercalators (planar aromatic moiety and basic center), and they were tested as antimicrobial, anti-QS and anticancer agents. To scout the mode of action of the new compounds, their DNA-binding affinity was assessed. Additionally, molecular docking was studied to substantiate the binding affinity of the new analogs toward DNA. Structure-activity relationship of the new pyrazolopyridines **2–9** was also studied, and it will smoothen the road for invention of new agents with distinguished effectiveness.

2. Results and discussion

2.1. Chemistry

Preparation of the new pyrazolo[3,4-*b*]pyridines **2–9** was described in Scheme 1. *Ortho* aminoester **1** was synthesized adopting the literature method [43]. Reaction of **1** with phthalic anhydride or succinic anhydride in refluxing glacial acetic acid produced ethyl 6-(1,3-dioxoisoindolin-2-yl)pyrazolopyridine-5-carboxylate **2** and 6-(2,5-dioxopyrrolidin-1-yl)pyrazolopyridine-5-carboxylate **3**, respectively. Heating **1** with ethyl acetoacetate or ethyl cyanoacetate in glacial acetic acid gave the oxobutanamide **4** and cyanoacetamide **5**, respectively. The (cyanomethyl)amine **6** was prepared *via* reaction of **1** with chloroacetonitrile in refluxing acetone and in presence of K_2CO_3 as a catalyst. On the other hand, the acetamide derivative **7** was attained through refluxing **1** in excess acetic anhydride. Heating **1** with the appropriate benzoyl chloride in acetone using K_2CO_3 as a catalyst gave the benzoylamines **8a,b**. Finally, refluxing **1** with the appropriate phenacyl bromide in acetone and in presence of K_2CO_3 as a catalyst afforded the 6-(2-(4-(un)substituted phenyl)-2-oxoethylamino)pyrazolopyridines **9a-c**.

2.2. Biology

2.2.1. Antimicrobial and antiquorum-sensing evaluation

Antimicrobial activity of the synthesized compounds was evaluated over Gram-negative bacteria (*Escherichia coli* ATCC 12435 and *Pseudomonas aeruginosa* PA01), Gram-positive bacteria (*Staphylococcus aureus* ATCC 29213 and *Bacillus cereus* UW 85) and fungi (*Candida albicans*, *Aspergillus fumigatus* 293 and *Aspergillus flavus* 3375). Minimal concentrations of compounds which prevent visible bacterial and fungal growth (MICs, μg/mL and μM) were set adopting the two-fold serial dilution method [44–48].

Compound **2** exhibited prominent and extended-spectrum

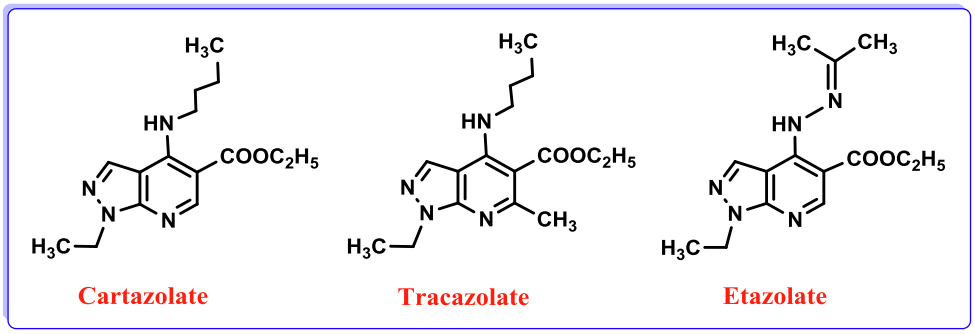

Fig. 2. Examples of marketed pyrazolopyridine drugs.

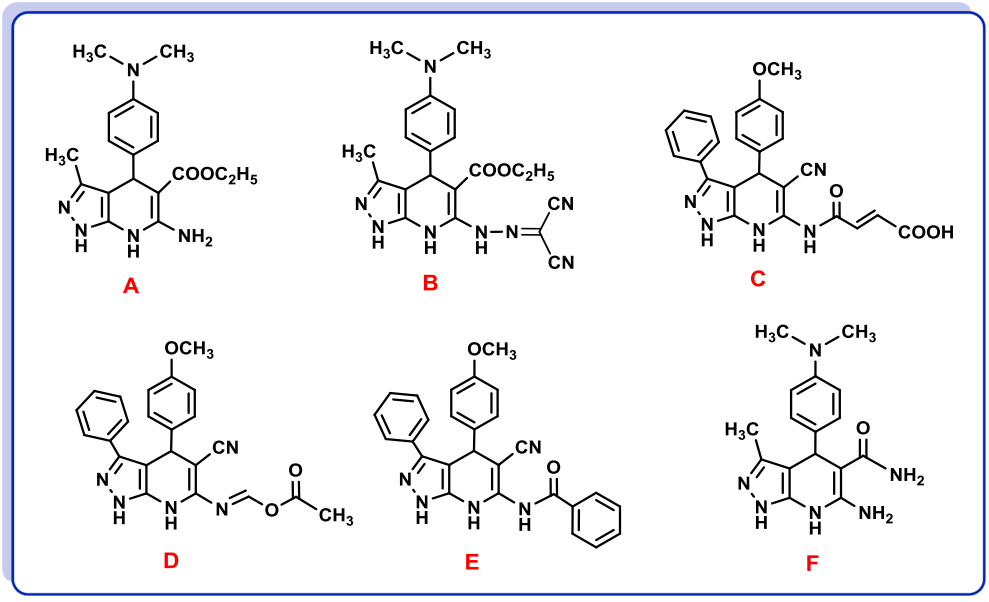

Fig. 3. Pyrazolopyridines with reported anticancer efficacy and DNA-binding affinity.

antimicrobial activity. Additionally, **2** was evidenced to be of higher potency than the effective pyrazolopyridines **J, N** and **O** that were synthesized in our previous study [25] toward all chosen microbial strains. Further, **2** was proved to be more potent than pyrazolopyridine **I** [25] toward *E coli* and *C. albicans*, and to be equipotent with it over *P. aeruginosa*, *S. aureus, B. cereus, A. fumigatus* and *A. flavus*. Moreover, **6** and **9c** displayed remarkable and extended-spectrum antibacterial activity. On the other hand, **3** and **9b** showed interesting efficacy toward Gram-positive bacteria. Further, **8b** exerted good selectivity over *P. aeruginosa*, *S. aureus* and *B. cereus*, whereas **7** illustrated good selectivity over *E. coli*, *S. aureus* and *B. cereus* (Table 1). The remaining compounds were either weakly active or inactive over the chosen microrganisms. Ampicillin (antibacterial drug) and fluconazole (antifungal drug) were used for comparison.

The new members were also tested for anti-QS activity over *Chromobacterium violaceum* ATCC 12472 [44,45,49] employing indole as a standard agent.

Acyl-homoserine lactones are signals produced by QS system of *C. violaceum*, and they adjust the freeing of a purple pigment (violacein) that induces QS communication among bacteria [50,51]. QS inhibition in *C. violaceum* will hinder the freeing of violacein, and it is defined by subtracting bacterial growth inhibition radius (r_1) from the total growth and pigment inhibition radius (r_2); consequently, QS inhibition = ($r_2 - r_1$) in mm. Results (Table 2) manifested that compound **9c** has strong effectiveness, while **2, 8b** and **9b** were moderately active. The remaining compounds were either weakly active or inactive.

2.2.1.1. Analysis of structure-activity relationship

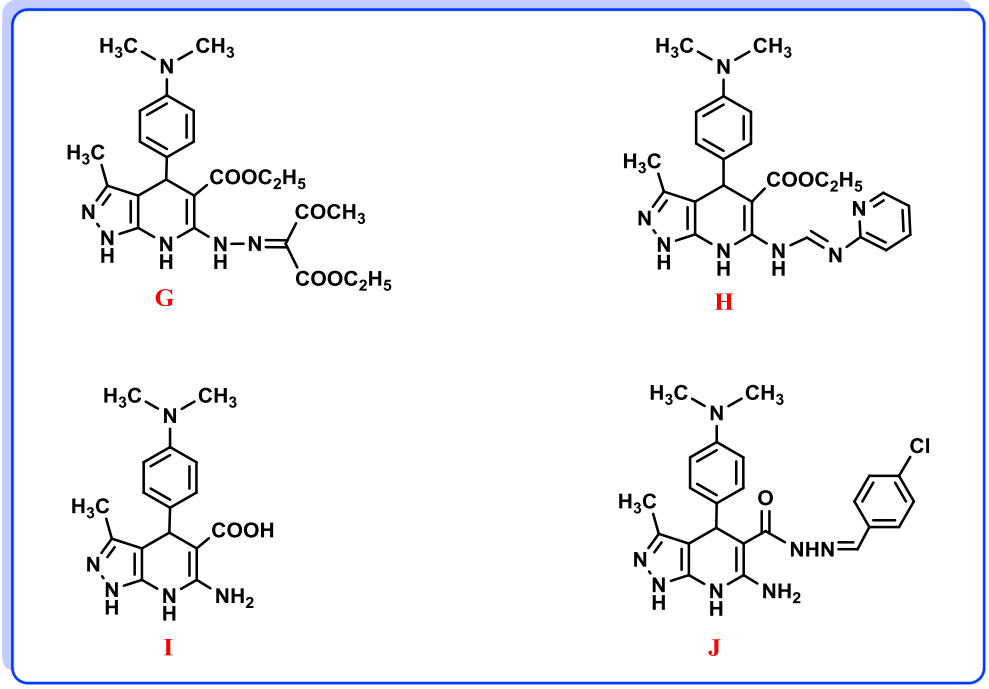

Fig. 4. Pyrazolopyridines with reported antimicrobial efficacy and DNA-binding affinity.

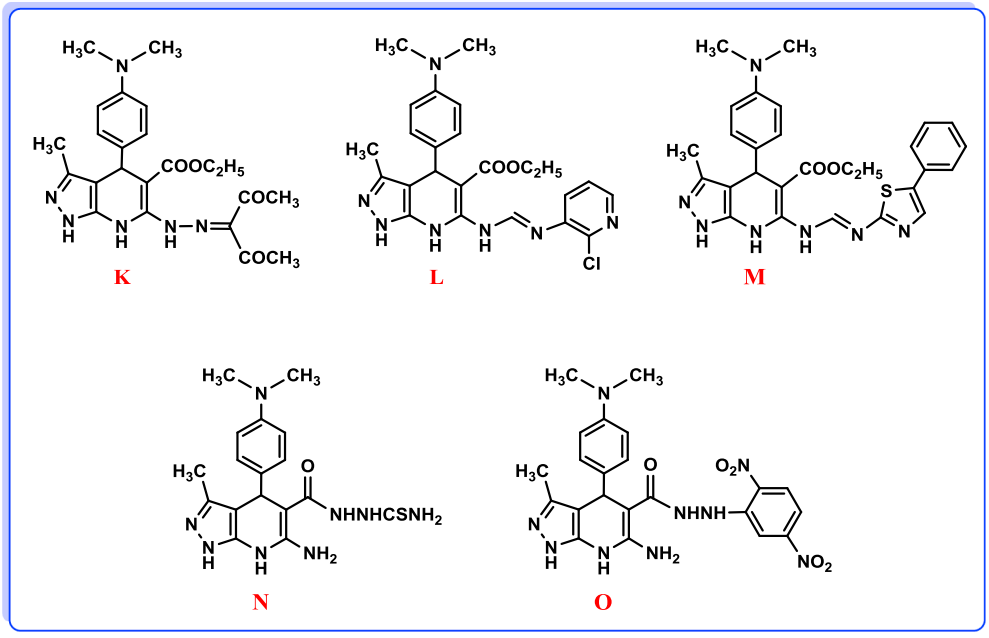

Fig. 5. Pyrazolopyridines with reported antimicrobial and anticancer efficacies as well as DNA-binding affinity.

*2.2.1.1.1. Referring to analogs **2** and **3**.* Introduction of 1,3-dioxoisoindolin-2-yl at 6-position of pyrazolopyridine skeleton gave rise to prominent activity over all screened microbial strains (compound **2**). Replacing 1,3-dioxoisoindolin-2-yl moiety in **2** with 2,5-dioxopyrrolidin-1-yl gave rise to reduced activity over all inspected microbes (compound **3** versus **2**), and this might be due to decreased lipophilicity in **3** (logP = 0.82) compared to **2** (logP = 3.60).

*2.2.1.1.2. In regard to compounds **4–7**.* The lipophilicity of compounds **4–7** affects their activity toward Gram-positive bacteria and *P. aeruginosa*, where increasing the lipophilicity led to improved activity, the activity order is **6** (logP = 1.31) > **7** (logP = 0.89) > **4** (logP = 0.66) > **5** (logP = 0.30).

*2.2.1.1.3. With respect to analogs **8a,b** and **9a-c**.* Presence of unsubstituted benzamido substituent at 6-position of pyrazolopyridine nucleus gave compound **8a** with acceptable activity on all examined bacteria, and weak antifungal activity toward the three chosen fungi. Exchanging unsubstituted benzamido with 4-nitrobenzamido led to augmented activity on all chosen microbes (compound **8b** versus **8a**), and this might be ascribed to existence of additional sites of hydrogen bonding interactions in **8b**. Besides, presence of 2-(4-bromophenyl)-2-oxoethylamino substituent at 6-position of pyrazolopyridine skeleton gave compound **9c** with outstanding effectiveness on all tested bacteria as well as moderate antifungal activity toward the three chosen fungi. Exchanging 4-bromophenyl moiety in **9c** with 4-chlorophenyl counterpart led to compound **9b** with decreased effectiveness on all examined microbial strains. Moreover, exchanging 4-chlorophenyl in **9b** with unsubstituted phenyl gave rise to **9a** with diminished antibacterial and abolished antifungal activities, and this might be related to the decreased lipophilicity of **9a** (logP = 2.67) compared to **9b** (logP = 3.35) and **9c** (logP = 3.48).

2.2.2. *In vitro anticancer evaluation*

The prepared compounds were evaluated for *in vitro* anticancer efficacy over liver (HepG2), breast (MCF-7) and cervix (Hela) cancer cells following MTT assay protocol [52–54]. DOX was employed for comparison. The compound's concentration needed to inhibit proliferation of 50% of cancer cells (IC_{50}, mean ± standard deviation (SD), μM) was set. The obtained results (Table 3) indicated that **2** and **9c** have potent and extended-spectrum activity, and the two compounds were substantiated to be more active than the pyrazolopyridines **A** [24], **F** [25] and **M** [24] that were synthesized in our previous work. Besides, the efficacy of the two analogs was much greater than that of the previously prepared pyrazolopyridines **C** [16], **D** [16] and **E** [16] toward HepG2 and MCF-7. Further, **8a, 8b** and **9b** showed promising activity toward the tested cancer cells. Additionally, **3** demonstrated interesting activity toward the three cancer cells, whereas **6** and **7** manifested interesting activity toward MCF-7 cells. The remaining compounds were proved to be moderately to weakly active toward the chosen cancer cells.

2.2.2.1. Analysis of structure-activity relationship

*2.2.2.1.1. Referring to analogs **2** and **3**.* Introduction of 1,3-dioxoisoindolin-2-yl at 6-position of pyrazolopyridine skeleton gave rise to outstanding activity over all tested cancer cells (compound **2**). Exchanging 1,3-dioxoisoindolin-2-yl moiety in **2** with 2,5-dioxopyrrolidin-1-yl gave rise to lowered activity on the screened cancer cells (compound **3** versus **2**), and this might be pertaining to reduced lipophilicity in **3** (logP = 0.82) compared to **2** (logP = 3.63).

*2.2.2.1.2. Taking into account analogs **4–7**.* The lipophilicity of compounds **4–7** has great influence on their anticancer activity, increasing the lipophilicity led to increased activity over the three cancer cells, the activity order is **6** (logP = 1.31) > **7** (logP = 0.89) > **4** (logP = 0.66) > **5** (logP = 0.30).

*2.2.2.1.3. With respect to analogs **8a,b** and **9a-c**.* The lipophilicity of **8a,b** and **9a-c** affect their anticancer activity, increasing the lipophilicity led to augmented activity, the activity order for compounds **8a,b** is **8a** (logP = 2.56) > **8b** (logP = 2.52), and for **9a-c** is **9c** (logP = 3.48) > **9b** (logP = 3.35) > **9a** (logP = 2.67).

2.2.3. *In vivo anticancer evaluation*

In vivo anticancer efficacy of compounds **2, 8a, 8b, 9b** and **9c** (with promising *in vitro* anticancer activity) was evaluated toward Ehrlich ascites carcinoma (EAC) in mice [55–57]. Mean survival time (MST) and % increase in lifespan (% ILS) of mice carrying EAC were set. Compounds **2** and **9c** demonstrated notable ILS of mice carrying EAC (Table 4). Viable EAC cell count and tumor volume were set, whereas **2** and **9c** demonstrated lucid drop in the count of viable EAC cells and tumor volume (Table 5). Effect on blood parameters of mice carrying EAC was studied (Table 6), whereas **2, 8a** and **9c** demonstrated higher hemoglobin (Hb) and RBCs count, and lower WBCs count than DOX (reference drug).

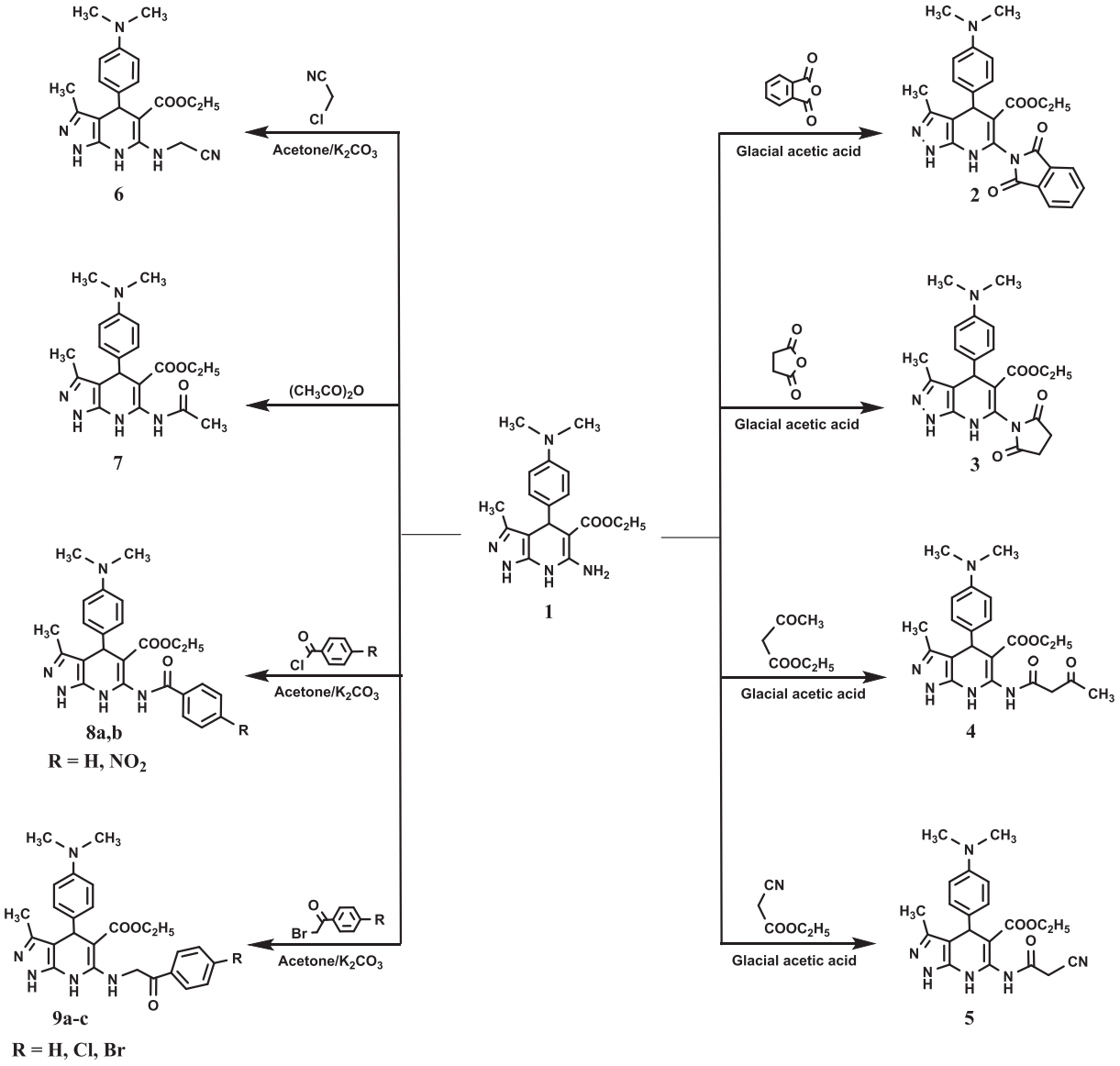

Scheme 1. Synthetic pathways of compounds **2–9**.

Table 1
MIC values of the target compounds toward the selected microorganisms.

Comp. No.	MIC, μg/mL (μM)[a]						
	E.coli	*P.aeruginosa*	*S. aureus*	*B. cereus*	*C. albicans*	*A. fumigatus*	*A. flavus*
2	**31.25 (66.31)**	**62.50 (132.55)**	**31.25 (66.31)**	**31.25 (66.31)**	**125 (265.10)**	**125 (265.10)**	**125 (265.10)**
3	250 (590.36)	250 (590.36)	**125 (295.10)**	**125 (295.10)**	500 (1180.72)	500 (1180.72)	1000 (2361.44)
4	**125 (293.78)**	500 (1175.12)	250 (587.56)	250 (587.56)	1000 (2350.23)	1000 (2350.23)	1000 (2350.23)
5	500 (1224.11)	500 (1224.11)	500 (1224.11)	500 (1224.11)	1000 (2448.22)	500 (1224.11)	500 (1224.11)
6	**125 (328.56)**	**62.50 (164.28)**	**62.50 (164.28)**	**62.50 (164.28)**	500 (1314.23)	500 (1314.23)	500 (1314.23)
7	**125 (325.99)**	250 (651.97)	**125 (325.99)**	**125 (325.99)**	500 (1303.95)	500 (1303.95)	500 (1303.95)
8a	500 (1123.59)	500 (1123.59)	500 (1123.59)	250 (561.79)	1000 (2247.19)	1000 (2247.19)	1000 (2247.19)
8b	250 (509.66)	**125 (254.83)**	**125 (254.83)**	**125 (254.83)**	500 (1019.33)	500 (1019.33)	500 (1019.33)
9a	500 (1087.76)	1000 (2175.52)	1000 (2175.52)	1000 (2175.52)	–	–	–
9b	250 (506.07)	250 (506.07)	**125 (253.04)**	**125 (253.04)**	500 (1012.15)	1000 (2024.29)	1000 (2024.29)
9c	**31.25 (58.04)**	**62.50 (116.07)**	**62.50 (116.07)**	**62.50 (116.07)**	500 (928.59)	500 (928.59)	500 (928.59)
Ampicillin	10 (28.6)	–	250 (715.5)	500 (1431)	NG	NG	NG
Fluconazole	NG	NG	NG	NG	2000 (6530.16)	–	–

[a] -, MIC > 2000 μg/mL.
MICs (μM) are exhibited between brackets.
NG: not given.
Bold values clarify the perfect results.

Table 2
Quorum-sensing inhibition by the target compounds.

Comp. No.	Pigment inhibition diameter (mm)[a]
	C. violaceum
2	11
3	4
4	–
5	–
6	9
7	9
8a	3
8b	11
9a	6
9b	11
9c	17
Indole	15

[a] Pigment inhibition diameter (mm): > 15 (strongly active); 10–15 (moderately active); 2–9 (weakly active); –, < 2 mm (inactive).

Table 3
Anticancer activity of the target compounds toward the selected cancer cells.

Comp. No.	IC_{50} (μM)[a,b]		
	HepG2	MCF-7	Hela
2	**3.63 ± 0.3**	**3.11 ± 0.2**	**4.91 ± 0.5**
3	**20.25 ± 1.6**	**20.41 ± 1.6**	**18.74 ± 1.4**
4	35.49 ± 2.2	43.78 ± 2.4	47.26 ± 2.6
5	54.32 ± 2.6	59.53 ± 2.8	59.37 ± 2.8
6	21.55 ± 1.7	**18.23 ± 1.5**	26.15 ± 1.9
7	26.37 ± 1.8	**20.58 ± 1.6**	38.57 ± 2.3
8a	**8.48 ± 0.8**	**9.74 ± 1.0**	**7.00 ± 0.8**
8b	**9.61 ± 0.9**	**10.43 ± 0.9**	**12.35 ± 1.1**
9a	58.32 ± 2.6	62.71 ± 2.9	47.52 ± 2.4
9b	**7.23 ± 0.8**	**7.67 ± 0.8**	**10.11 ± 0.9**
9c	**4.24 ± 0.3**	**4.06 ± 0.5**	**4.22 ± 0.5**
DOX	4.30 ± 0.2	3.97 ± 0.2	5.17 ± 0.4

[a] IC_{50} = mean ± SD of three experiments.
[b] IC_{50} (μM): 1–20 (strongly active); 21–50 (moderately active); 51–100 (weakly active); > 100 (inactive).
Bold values clarify the perfect results.

Table 4
Effect of **2**, **8a**, **8b**, **9b** and **9c** on MST and % ILS of mice carrying EAC.

Group	MST (day)[a]	% ILS
Normal	NG	NG
EAC only	18	NG
2	**68**	**277.8**
8a	58	222.2
8b	41	127.8
9b	49	172.2
9c	**66**	**266.7**
DOX	62	244.4

[a] Values = mean of three experiments.
NG: not given.
Bold values clarify the perfect results.

2.2.4. Cytotoxicity evaluation against normal cells

Analogs **2, 8a, 8b, 9b** and **9c** were checked for cytotoxicity against WISH amnion epithelial and W138 lung fibroblast normal cells [52–54]. IC_{50} values of the active compounds and DOX (cytotoxic drug) were set (Table 7). The examined analogs were evidenced to be more safe than DOX on the two normal cells.

2.2.5. DNA-binding evaluation

Targeting DNA is the mode of action of lots of antimicrobial and anticancer agents, including pyrazolo[3,4-*b*]pyridines [16,24,25].

Table 5
Effect of **2**, **8a**, **8b**, **9b** and **9c** on viable EAC cell count and tumor volume.

Group	Viable cell count (10^6/mL)[a]	Tumor volume (mL)[a]
Normal	NG	NG
EAC only	77.41	10.15
2	**18.44**	**1.15**
8a	21.38	1.35
8b	34.37	2.25
9b	30.86	1.65
9c	**17.57**	**1.10**
DOX	16.36	1.00

[a] Values = mean of three experiments.
NG: not given.
Bold values clarify the perfect results.

Table 6
Effect of **2**, **8a**, **8b**, **9b** and **9c** on blood parameters of mice carrying EAC.

Group	Hb (g/dl)[a]	RBCs (10^6/mm^3)[a]	WBCs (10^3/mm^3)[a]
Normal	13.85	6.21	5.49
EAC only	7.05	3.59	20.53
2	**13.96**	**5.89**	**7.11**
8a	**13.45**	**5.55**	**8.84**
8b	12.11	5.10	10.18
9b	12.55	5.18	9.05
9c	**13.52**	**5.62**	**8.39**
DOX	12.75	5.32	8.96

[a] Values = mean of three experiments.
Bold values clarify the perfect results.

Table 7
IC_{50} values of **2**, **8a**, **8b**, **9b** and **9c** toward the selected normal cells.

Comp. No.	IC_{50} (μM)[a,b]	
	WISH	W138
2	64.58 ± 3.9	53.96 ± 3.1
8a	58.66 ± 3.7	61.37 ± 3.8
8b	68.53 ± 4.1	72.55 ± 4.3
9b	60.07 ± 3.9	74.52 ± 4.4
9c	55.61 ± 3.6	60.31 ± 3.8
DOX	8.14 ± 0.9	6.68 ± 0.5

[a] IC_{50} = mean ± SD of three experiments.
[b] IC_{50} (μM): 1–20 (strongly active); 21–50 (moderately active); 51–100 (weakly active); > 100 (not cytotoxic).

Subsequently, the active members in the present research were assessed for their ability to interact with DNA [58].

Methyl green/DNA displacement assay [58] is important in assessment of the ability of DNA-binding agents to displace methyl green from DNA. Concentrations of **2, 3, 6, 7, 8a, 8b, 9b, 9c** and DOX (positive control) that cause the absorbance of methyl green/DNA complex to be reduced by half (IC_{50}, μM) were set. Results (Table 8) demonstrated that **2, 3, 8b, 9b** and **9c** have strong affinity to DNA in comparison to DOX. Besides, the five candidates were proved to have better affinity (IC_{50} = 27.13–31.78 μM) than the previously synthesized pyrazolopyridines **A** [24], **C** [16], **D** [16], **E** [16], **K** [24], **N** [25] and **O** [25] (IC_{50} = 32.38–82.82 μM). Further, **6, 7** and **8a** displayed moderate affinity (IC_{50} = 43.52–48.69 μM). Thus, the eight active compounds are foreseen to act *via* interaction with DNA.

3. *In silico* studies

3.1. Molecular modeling

With the aim of examining the potential DNA-binding mode of the synthesized compounds with promising antimicrobial and anticancer

Table 8
DNA-binding evaluation of the active members.

Comp. No.	Methyl green/DNA IC_{50} (μM)[a]
2	**27.13 ± 1.1**
3	**31.78 ± 1.2**
6	48.69 ± 2.1
7	43.52 ± 1.9
8a	46.78 ± 1.9
8b	**29.58 ± 1.2**
9b	**31.78 ± 1.2**
9c	**29.15 ± 1.1**
DOX	31.27 ± 1.2

[a] IC_{50} = mean ± SD of three experiments.
Bold values clarify the perfect results.

Table 9
Binding energies and hydrogen bonding of the active members to DNA sequence d(CGATCG).

Comp. No.	Binding energy (kcal/mol)	No. of H-bonds
2	**−25.3**	2
3	−20.4	2
6	−17.3	1
7	−16.4	1
8a	−18.4	1
8b	−19.1	2
9b	−21.1	2
9c	**−21.5**	2
DOX	−35.9	7

Bold values clarify the perfect results.

activities **2**, **3**, **6**, **7**, **8a, 8b, 9b** and **9c**, molecular docking studies based on the crystal structure of DOX with (DNA sequence d(CGATCG), PDB code: 1D12) was performed using Molegro 2.5 software [59]. As shown in Fig. 6, the binding mode of DOX to the DNA sequence d(CGATCG) features intercalation of the tetracyclic planar ligand between cytosine 5 and guanine 6 residues. In addition, the sugar moiety of DOX is involved in six hydrogen bonds with the DNA sequence (Fig. 6). The binding free energies of the best docking pose of the tested compounds and DOX to the DNA sequence are listed in Table 9. The compounds exhibited binding energies to the DNA sequence in the range of −16.4 to −25.3 kcal/mol in comparison to a binding energy of −35.9 kcal/mol for DOX. Consistent with the results of antibacterial, anticancer and DNA-binding assays, compounds **2** and **9c** exhibited the strongest binding to the DNA sequence with binding energy values of −25.3 and −21.5 kcal/mol, respectively. Similarly to DOX, all the tested compounds displayed intercalation between cytosine 5 and guanine 6 residues of the DNA sequence. Moreover, each compound possessed at least one hydrogen bond to the DNA sequence (Table 9).

The 3D interactions of **2** and **9c** with the DNA sequence d(CGATCG) are displayed in Figs. 7A and 8A, respectively. Moreover, Lead IT 2.3.2 software [60] was utilized to create 2D binding poses of **2** and **9c** to the DNA sequence (Figs. 7B and 8B, respectively). As shown in the binding interaction of **2** with the DNA sequence (Fig. 7), 1,3-dioxoisoindolin-2-yl moiety of **2** is involved in hydrophobic interaction in the binding site upon intercalation between cytosine 5 and guanine 6 residues of the DNA sequence. In addition, pyrazolo[3,4-*b*]pyridine and 1,3-dioxoisoindolin-2-yl scaffolds in **2** featured two key hydrogen bonding interactions with water molecules in the binding site of the target. Based on the 3D and 2D binding poses of **9c** to the DNA sequence, 4-(dimethylamino)phenyl and ethyl ester of **9c** featured hydrophobic interaction with cytosine 5 and guanine 6 residues (Fig. 8). Similarly to **2**, compound **9c** possessed two hydrogen bonding interactions with water molecules of the target through ester and ketone functional groups in **9c**. Ultimately, molecular docking studies presented a preliminary conception of the mode of binding of the new members. Identification of the pharmacophoric features of the active members in this research is crucial for further structural optimization aiming at higher binding affinity to DNA and more potent antimicrobial and anticancer activities. 3D and 2D pharmacophoric maps for **2** and **9c** (Figs. 9 and 10, respectively) were constructed by LigandScout 4.1 software [61]. The proper pharmacophoric features include hydrogen bond donors and acceptors, ionizable regions and lipophilic areas.

3.2. Prediction of Lipinski's rule parameters, carcinogenicity and drug score

Computational studies are advantageous in prediction of toxicity, pharmacokinetics and physicochemical characters of new compounds [62]. Aqueous solubility and lipophilicity are the major determinants of drug absorption. Hence, the new candidates were analyzed for expectancy of Lipinski's rule parameters [63,64] and Veber's standards [64,65]. Besides, their carcinogenicity [66], solubility and drug score [67] were predicted. Detailed results are described in the

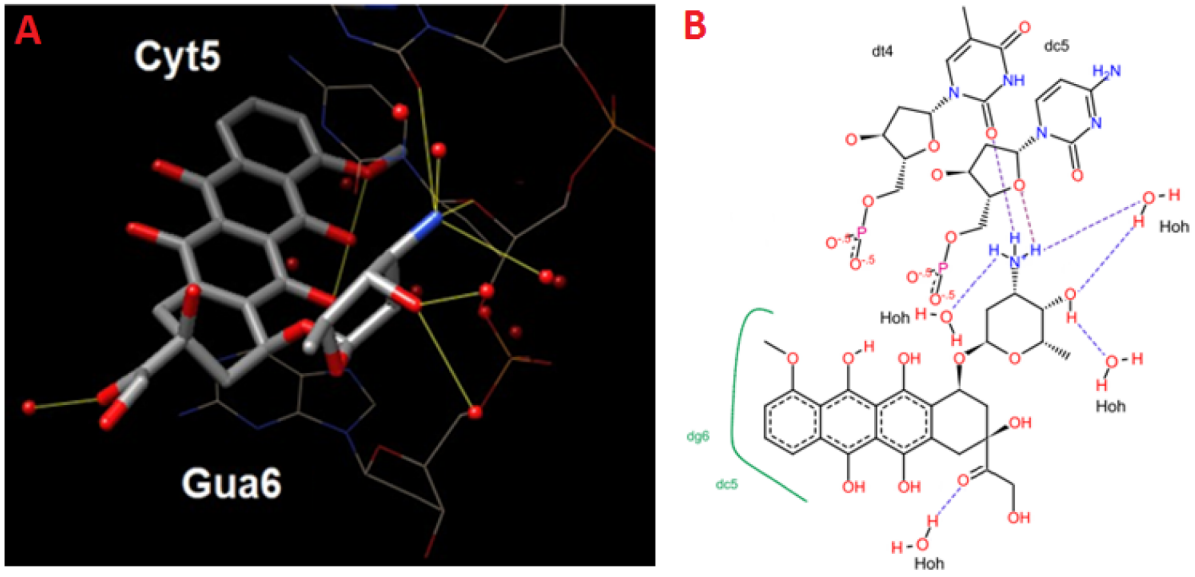

Fig. 6. (A) 3D Interaction of DOX with DNA sequence d(CGATCG). Atoms are colored as following: blue for nitrogen atoms, red for oxygen atoms and grey for carbon atoms. **(B)** 2D Interaction of DOX with DNA sequence d(CGATCG). Dashed lines point to hydrogen bonds and green solid lines point to hydrophobic interactions.

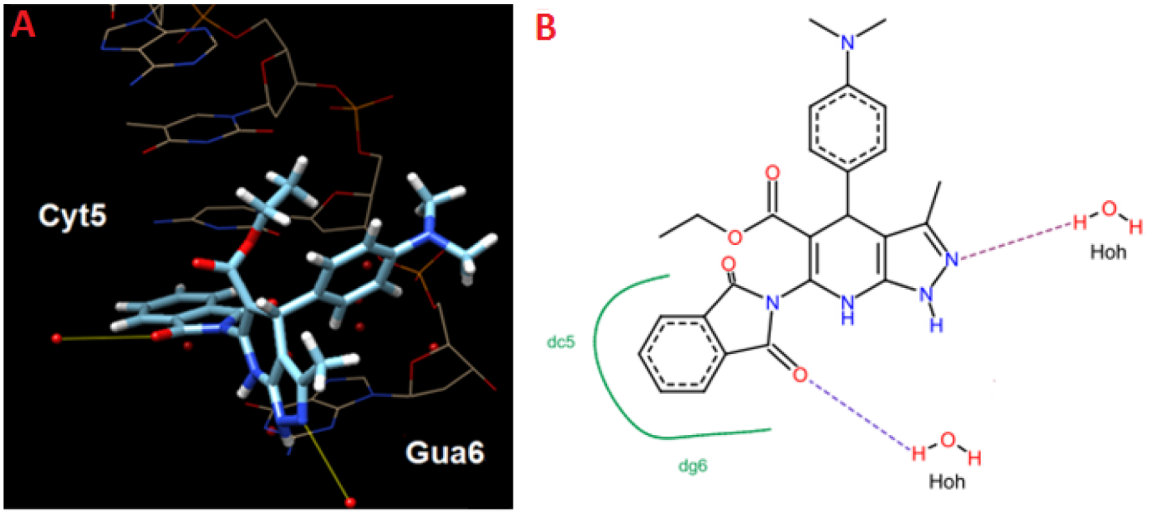

Fig. 7. (A) 3D Interaction of **2** with DNA sequence d(CGATCG). Atoms are colored as following: blue for nitrogen atoms, white for hydrogen atoms, red for oxygen atoms and cyan for carbon atoms. **(B)** 2D Interaction of **2** with DNA sequence d(CGATCG). Dashed lines point to hydrogen bonds and green solid lines point to hydrophobic interactions.

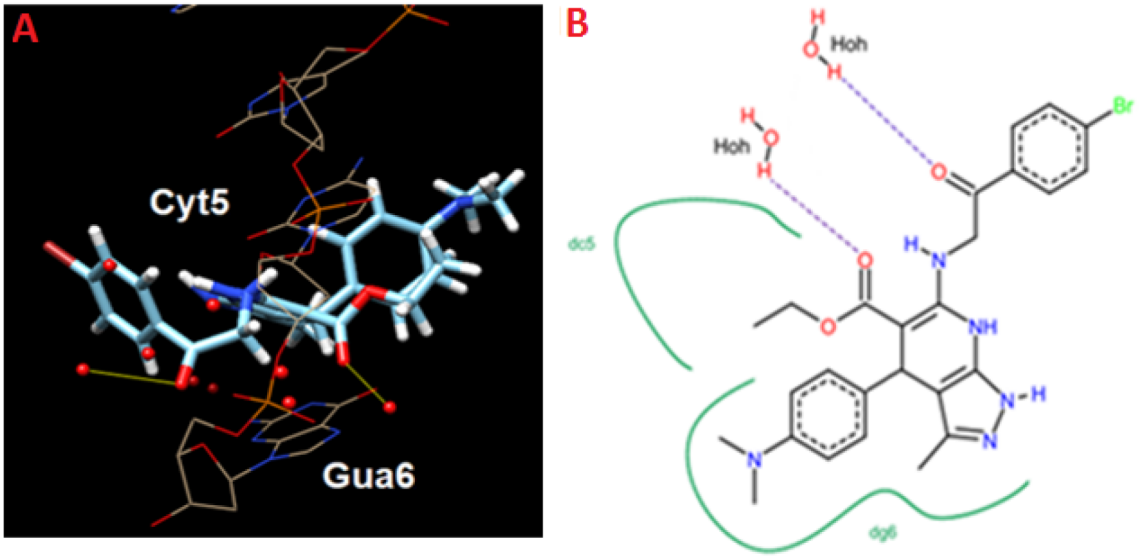

Fig. 8. (A) 3D Interaction of **9c** with DNA sequence d(CGATCG). Atoms are colored as following: blue for nitrogen atoms, white for hydrogen atoms, red for oxygen atoms, dark red for bromine and cyan for carbon atoms. **(B)** 2D Interaction of **9c** with DNA sequence d(CGATCG). Dashed lines point to hydrogen bonds and green solid lines point to hydrophobic interactions.

Supplementary File.

4. Conclusion

New pyrazolopyridines with promising antimicrobial and anticancer activities were discovered in the current research. Results demonstrated that compound **2** has potent and extended-spectrum antimicrobial activity. Further, **6** and **9c** demonstrated interesting antibacterial effectiveness on all tested bacteria. Additionally, **9c** showed strong anti-QS activity, whereas **2** exhibited moderate activity, and the two compounds might be utilized as eminent and extended-spectrum antibacterial agents with decreased hazard of bacterial resistance. With respect to anticancer assessment, results revealed that **2** and **9c** have potent efficacy toward all tested cancer cells. Likewise, **8a, 8b** and **9b** showed excellent efficacy toward the three cell lines. Moreover, the five potent anticancer derivatives **2, 8a, 8b, 9b** and **9c** were proved to be of lower cytotoxicity than DOX against the tested normal cells. Further, **2** and **9c** demonstrated the greatest activity over EAC in mice. Generally talking, analogs **2** and **9c** might be utilized as powerful and selective anticancer agents with reduced peril of microbial infections. DNA-binding evaluation indicated that **2, 3, 8b, 9b** and **9c** have strong affinity, whereas **6, 7,** and **8a** manifested moderate binding, and the eight analogs are foreseen to act through targeting DNA. Additionally, docking studies propped the efficacious binding of **2** and **9c** to DNA. *In silico* studies underlined that the new members are prophesied to manifest excellent intestinal absorption. An overview on the attained results asserted that rational design of the new pyrazolopyridines of potential antimicrobial and anticancer efficacies was appropriate, and it gave rise to development of new candidates with enhanced efficacies in comparison to the pyrazolopyridines **A, F, J, M, N** and **O** that were prepared in our previous studies [24,25]. The most effective members **2** and **9c** could be considered as propitious lead compounds for future optimization in order to get new more active members.

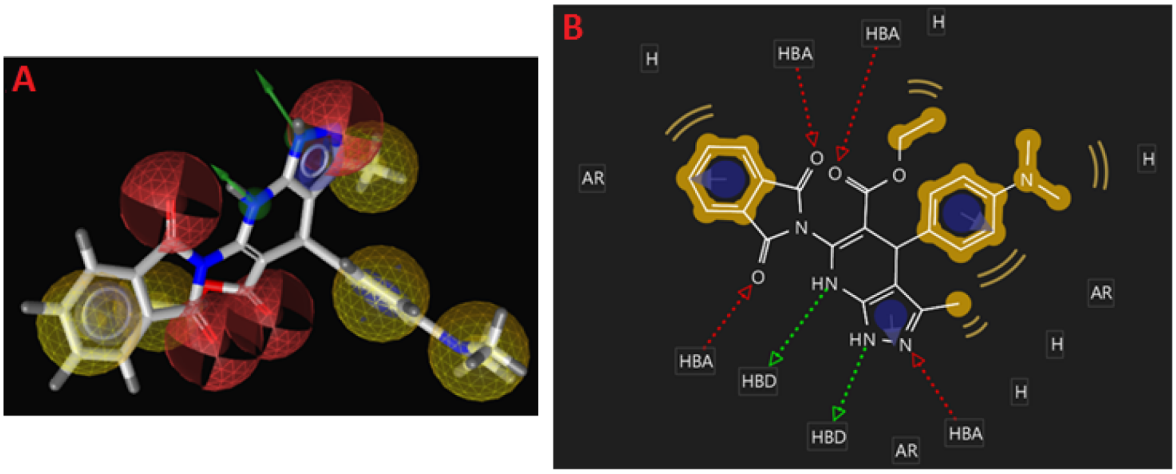

Fig. 9. (A) 3D Pharmacophoric map of **2**; color coding is red for hydrogen acceptors, green for hydrogen donors and yellow for hydrophobic regions. **(B)** 2D Pharmacophoric map of **2**; HBA is hydrogen bond acceptor, HBD is hydrogen bond donor, H is hydrophobic center and AR is aryl.

5. Experimental section

Stuart (SMP30) melting point apparatus was utilized to measure melting points ˚C. Unicam SP 1000 IR spectrometer was used to record IR spectra (KBr, ν in cm^{-1}). Bruker 500 MHz spectrometer was utilized to record ^{1}H and ^{13}C NMR spectra in DMSO-d_6. Mass spectra were acquired on JEOL JMS-600H spectrometer (70 eV). Elemental analyses (% C, H, N) were done and they were in conformity with the suggested structures within ± 0.4% of theoretical values. Times of reactions were regulated by TLC (silica gel 60 F254), and spots were detected using UV (366 nm). Elution was achieved using chloroform/methanol (9:1). *Ortho* aminoester **1** was prepared taking on the previous method [43]. *E. coli*, *P. aeruginosa*, *S. aureus*, *B. cereus*, and *C. albicans* were attained from Microbiology Department, Faculty of Pharmacy, Mansoura University, Egypt. *A. fumigatus* and *A. flavus* were obtained from Prof. Nancy Keller, Medical Microbiology and Immunology Department, Wisconsin-Madison University, USA. *C. violaceum* was supplied by Prof. Bob Mclean, Biology Department, Texas State University, USA. Human cell lines and EAC cells were attained from VACSERA, Egypt. Adult male albino mice (weight: 20–25 g) were attained from Pharmacology Department, Faculty of Pharmacy, Mansoura University, Egypt, and they lived in microlon boxes at 25 ˚C with an orderly 12 h light/dark cycle.

5.1. Chemistry

5.1.1. Synthesis of compounds *2* and *3*

A mixture of *ortho* aminoester **1** (0.341 g, 1 mmol) and acid anhydride (1 mmol) in glacial acetic acid (10 mL) was refluxed for 20–24 h. The solvent was poured onto ice and the precipitate formed was filtered and crystallized from ethanol.

*5.1.1.1. Ethyl 4-(4-(dimethylamino)phenyl)-3-methyl-6-(1,3-dioxoisoindolin-2-yl)-4,7-dihydro-1H-pyrazolo[3,4-b]pyridine-5-carboxylate **(2)***. Yield 63%, m.p. 232–233 ˚C. IR: 3382, 3287 (2NH), 1785, 1732 (2C=O), 1715 (COOC$_2$H$_5$). ^{1}H NMR δ: 1.26 (t, 3H, J = 7.0 Hz, OCH$_2$CH$_3$), 1.94 (s, 3H, CH$_3$), 2.96 (s, 6H, N(CH$_3$)$_2$), 4.25–4.29 (q, 2H, J = 7.0 Hz, OCH$_2$CH$_3$), 5.16 (s, 1H, C$_4$-H), 6.75 (d, 2H, J = 8.0 Hz, Ar-H), 7.27 (d, 2H, J = 7.5 Hz, Ar-H), 7.56–7.87 (m, 4H, Ar-H), 8.78 (s, 1H, NH), 11.14 (s, 1H, NH). ^{13}C NMR δ: 12.1, 14.2, 35.7, 42.2, 62.0, 89.7, 110.3, 116.5, 125.8, 127.8, 131.8, 132.0, 136.0, 136.2, 147.9, 152.9, 154.2, 162.5, 173.6. Anal. Calcd for $C_{26}H_{25}N_5O_4$ (471.51).

*5.1.1.2. Ethyl 4-(4-(dimethylamino)phenyl)-3-methyl-6-(2,5-dioxopyrrolidin-1-yl)-4,7-dihydro-1H-pyrazolo[3,4-b]pyridine-5-carboxylate **(3)***. Yield 72%, m.p. 227–229 ˚C. IR: 3365, 3240 (2NH), 1791, 1734 (2C=O), 1719 (COOC$_2$H$_5$). ^{1}H NMR δ: 1.28 (t, 3H, J = 7.0 Hz, OCH$_2$CH$_3$), 1.73 (s, 3H, CH$_3$), 2.76 (s, 4H, 2CH$_2$), 2.97 (s, 6H, N(CH$_3$)$_2$), 4.25–4.29 (q, 2H, J = 7.0 Hz, OCH$_2$CH$_3$), 5.03 (s, 1H, C$_4$-H), 6.75 (d, 2H, J = 9.0 Hz, Ar-H),

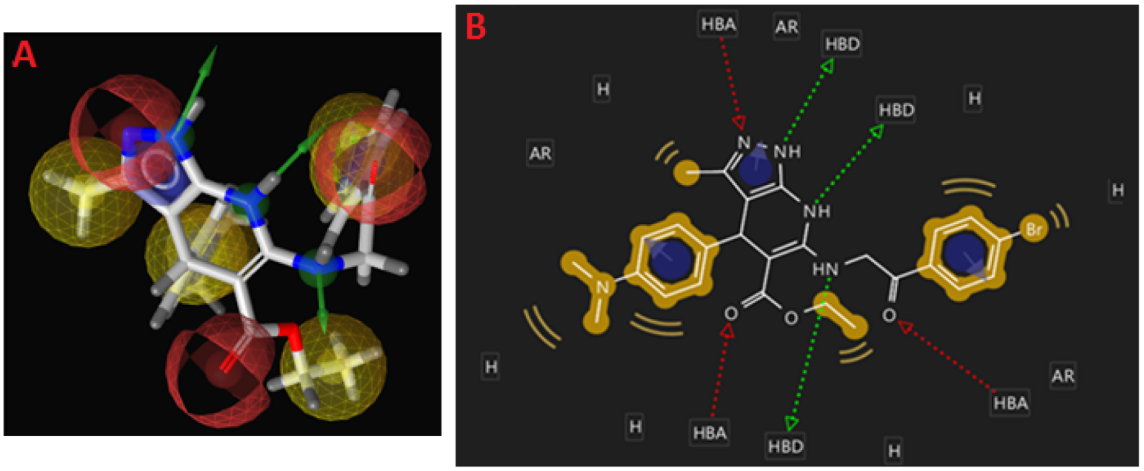

Fig. 10. (A) 3D Pharmacophoric map of **9c**; color coding is red for hydrogen acceptors, green for hydrogen donors and yellow for hydrophobic regions. **(B)** 2D Pharmacophoric map of **9c**; HBA is hydrogen bond acceptor, HBD is hydrogen bond donor, H is hydrophobic center and AR is aryl.

7.31 (d, 2H, J = 9.0 Hz, Ar-H), 9.78 (s, 1H, NH), 11.37 (s, 1H, NH). ^{13}C NMR δ: 12.0, 14.1, 27.4, 33.8, 40.0, 61.4, 87.9, 102.1, 111.7, 129.9, 131.4, 137.9, 148.6, 152.8, 154.1, 163.0, 163.5. MS m/z (%): 423 (1.28, M^+), 93 (100.00). Anal. Calcd for $C_{22}H_{25}N_5O_4$ (423.47).

*5.1.2. Synthesis of pyrazolopyridines **4** and **5***

A mixture of *ortho* aminoester **1** (0.341 g, 1 mmol) and ethyl acetoacetate or ethyl cyanoacetate (1 mmol) in glacial acetic acid (10 mL) was refluxed for 10–12 h. The solvent was concentrated and the precipitate formed was filtered and crystallized from dioxane to produce **4** and **5**, respectively.

*5.1.2.1. Ethyl 4-(4-(dimethylamino)phenyl)-3-methyl-6-(3-oxobutanamido)-4,7-dihydro-1H-pyrazolo[3,4-b]pyridine-5-carboxylate **(4)***. Yield 73%, m.p. 216–218 °C. IR: 3381, 3323, 3197 (3NH), 1725 (COOC$_2$H$_5$), 1687, 1656 (2C=O). ^{1}H NMR δ: 1.28 (t, 3H, J = 7.5 Hz, OCH$_2$CH$_3$), 1.93 (s, 3H, CH$_3$), 2.49 (s, 3H, CH$_3$), 3.07 (s, 6H, N(CH$_3$)$_2$), 3.65 (s, 2H, CH$_2$), 4.23–4.28 (q, 2H, J = 7.5 Hz, OCH$_2$CH$_3$), 4.85 (s, 1H, C$_4$-H), 6.75 (d, 2H, J = 7.5 Hz, Ar-H), 7.27 (d, 2H, J = 7.5 Hz, Ar-H), 8.31 (s, 1H, NH), 9.78 (s, 1H, NH), 10.65 (s, 1H, NH). ^{13}C NMR δ: 12.9, 13.9, 21.1, 34.1, 42.2, 51.1, 61.4, 85.4, 110.6, 116.1, 129.7, 130.8, 136.1, 148.8, 154.3, 159.5, 163.8, 169.9, 172.1. MS m/z (%): 425 (0.04, M^+), 69 (100.00). Anal. Calcd for $C_{22}H_{27}N_5O_4$ (425.48).

*5.1.2.2. Ethyl 6-(2-cyanoacetamido)-4-(4-(dimethylamino)phenyl)-3-methyl-4,7-dihydro-1H-pyrazolo[3,4-b]pyridine-5-carboxylate **(5)***. Yield 67%, m.p. 196–198 °C. IR: 3372, 3330, 3229 (3NH), 2216 (C≡N), 1709 (COOC$_2$H$_5$), 1666 (C=O). ^{13}C NMR δ: 11.2, 13.2, 25.4, 30.4, 42.1, 61.8, 89.0, 110.6, 117.1, 125.8, 130.6, 131.9, 136.3, 144.2, 154.4, 162.2, 165.7, 172.1. MS m/z (%): 410 (0.17, M^+ + 2), 409 (0.28, M^+ + 1), 408 (0.10, M^+), 93 (100.00). Anal. Calcd for $C_{21}H_{24}N_6O_3$ (408.45).

*5.1.3. Synthesis of ethyl 6-((cyanomethyl)amino)-4-(4-(dimethylamino) phenyl)-3-methyl-4,7- dihydro-1H-pyrazolo[3,4-b]pyridine-5-carboxylate **(6)***

A mixture of *ortho* aminoester **1** (0.341 g, 1 mmol), chloroacetonitrile (0.075 g, 1 mmol) and K_2CO_3 (0.207 g, 1.5 mol) in acetone (10 mL) was refluxed for 12 h. The mixture was filtered and the filtrate was evaporated. The attained product was crystallized from ethanol.

Yield 70%, m.p. 241–243 °C. IR: 3381, 3320, 3254 (3NH), 2211 (C≡N), 1716 (COOC$_2$H$_5$). ^{1}H NMR δ: 1.28 (t, 3H, J = 8.5 Hz, OCH$_2$CH$_3$), 2.13 (s, 3H, CH$_3$), 2.96 (s, 6H, N(CH$_3$)$_2$), 3.98 (s, 2H, CH$_2$), 4.25–4.29 (q, 2H, J = 9.0 Hz, OCH$_2$CH$_3$), 4.89 (s, 1H, C$_4$-H), 6.83 (d, 2H, J = 9.0 Hz, Ar-H), 7.24 (d, 2H, J = 8.5 Hz, Ar-H), 8.56 (s, 1H, NH), 9.78 (s, 1H, NH), 11.29 (s, 1H, NH). ^{13}C NMR δ: 11.1, 14.6, 32.1, 36.1, 41.9, 60.9, 89.6, 110.6, 114.6, 115.1, 129.7, 131.9, 136.0, 147.8, 156.9, 165.0, 169.6. MS m/z (%): 381 (0.28, M^+ + 1), 216 (100.00). Anal. Calcd for $C_{20}H_{24}N_6O_2$ (380.45).

*5.1.4. Synthesis of ethyl 6-acetamido-4-(4-(dimethylamino)phenyl)-3-methyl-4,7-dihydro-1H-pyrazolo[3,4-b]pyridine-5-carboxylate **(7)***

A mixture of *ortho* aminoester **1** (0.341 g, 1 mmol) and acetic anhydride (5 mL) was refluxed for 6 h. The mixture was evaporated and the remained residue was crystallized from dioxane.

Yield 62%, m.p. 213–215 °C. IR: 3384, 3261 (3NH), 1718 (COOC$_2$H$_5$), 1673 (C=O). ^{1}H NMR δ: 1.27 (t, 3H, J = 6.5 Hz, OCH$_2$CH$_3$), 1.88 (s, 3H, CH$_3$), 2.18 (s, 3H, COCH$_3$), 2.97 (s, 6H, N(CH$_3$)$_2$), 4.26–4.28 (q, 2H, J = 6.5 Hz, OCH$_2$CH$_3$), 4.92 (s, 1H, C$_4$-H), 6.74 (d, 2H, J = 8.0 Hz, Ar-H), 7.26 (d, 2H, J = 8.5 Hz, Ar-H), 9.36 (s, 1H, NH), 9.78 (s, 1H, NH), 11.14 (s, 1H, NH). ^{13}C NMR δ: 11.9, 14.2, 25.0, 33.9, 42.1, 62.0, 89.7, 110.5, 117.9, 129.8, 132.0, 136.2, 147.9, 152.9, 154.2, 162.5, 173.6. MS m/z (%): 383 (0.1, M^+), 216 (100.00). Anal. Calcd for $C_{20}H_{25}N_5O_3$ (383.44).

*5.1.5. Synthesis of pyrazolopyridines **8a,b** and **9a-c***

A mixture of *ortho* aminoester **1** (0.341 g, 1 mmol), benzoyl chloride or phenacyl bromide derivatives (1 mmol) and K_2CO_3 (0.207 g, 1.5 mmol) in acetone (10 mL) was refluxed for 8–18 h. The mixture was filtered and the filtrate was evaporated. The attained residue was crystallized from dioxane to yield compounds **8a,b** and **9a-c**, respectively.

*5.1.5.1. Ethyl 6-benzamido-4-(4-(dimethylamino)phenyl)-3-methyl-4,7-dihydro-1H-pyrazolo[3,4-b]pyridine-5-carboxylate **(8a)***. Yield 69%, m.p. 222–224 °C. IR: 3340, 3265 (3NH), 1710 (COOC$_2$H$_5$), 1665 (C=O). ^{1}H NMR δ: 1.28 (t, 3H, J = 7.0 Hz, OCH$_2$CH$_3$), 1.89 (s, 3H, CH$_3$), 2.96 (s, 6H, N(CH$_3$)$_2$), 4.25–4.29 (q, 2H, J = 7.0 Hz, OCH$_2$CH$_3$), 4.87 (s, 1H, C$_4$-H), 6.76 (d, 2H, J = 7.5 Hz, Ar-H), 7.28 (d, 2H, J = 7.0 Hz, Ar-H), 7.87–8.09 (m, 5H, Ar-H), 8.39 (s, 1H, NH), 8.56 (s, 1H, NH), 9.78 (s, 1H, NH). ^{13}C NMR δ: 11.6, 13.7, 30.4, 41.9, 60.8, 86.0, 103.0, 110.6, 124.6, 128.5, 129.2, 130.6, 131.9, 134.7, 136.1, 148.8, 154.3, 155.1, 165.8, 169.6. MS m/z (%): 447 (0.44, M^+ + 1), 93 (100.00). Anal. Calcd for $C_{25}H_{27}N_5O_3$ (445.51).

*5.1.5.2. Ethyl 4-(4-(dimethylamino)phenyl)-3-methyl-6-(4-nitrobenzamido)-4,7-dihydro-1H-pyrazolo[3,4-b]pyridine-5-carboxylate **(8b)***. Yield 73%, m.p. 237–239 °C. IR: 3381, 3245, 3194 (3NH), 1721 (COOC$_2$H$_5$), 1666 (C=O). ^{1}H NMR δ: 1.26 (t, 3H, J = 7.0 Hz, OCH$_2$CH$_3$), 1.82 (s, 3H, CH$_3$), 2.96 (s, 6H, N(CH$_3$)$_2$), 4.25–4.29 (q, 2H, J = 7.5 Hz, OCH$_2$CH$_3$), 4.85 (s, 1H, C$_4$-H), 6.75 (d, 2H, J = 7.5 Hz, Ar-H), 7.27 (d, 2H, J = 7.5 Hz, Ar-H), 8.04 (d, 2H, J = 7.5 Hz, Ar-H), 8.20 (d, 2H, J = 7.0 Hz, Ar-H), 9.07 (s, 1H, NH), 9.78 (s, 1H, NH), 10.35 (s, 1H, NH). ^{13}C NMR δ: 10.9, 13.9, 35.1, 41.1, 61.4, 88.0, 110.6, 117.8, 125.8, 129.0, 129.1, 131.7, 138.0, 138.2, 148.8, 150.1, 154.3, 159.5, 163.8, 169.9. MS m/z (%): 491 (0.04, M^+), 57 (100.00). Anal. Calcd for $C_{25}H_{26}N_6O_5$ (490.51).

*5.1.5.3. Ethyl 4-(4-(dimethylamino)phenyl)-3-methyl-6-(2-oxo-2-phenyl ethylamino)-4,7-dihydro-1H-pyrazolo[3,4-b]pyridine-5-carboxylate **(9a)***. Yield 71%, m.p. 233–234 °C. IR: 3371, 3228, 3192 (3NH), 1725 (COOC$_2$H$_5$), 1687 (C=O). ^{1}H NMR δ: 1.29 (t, 3H, J = 7.5 Hz, OCH$_2$CH$_3$), 1.91 (s, 3H, CH$_3$), 2.97 (s, 6H, N(CH$_3$)$_2$), 4.24–4.28 (q, 2H, J = 7.5 Hz, OCH$_2$CH$_3$), 4.65 (s, 2H, CH$_2$), 4.93 (s, 1H, C$_4$-H), 6.67 (d, 2H, J = 7.5 Hz, Ar-H), 7.28 (d, 2H, J = 7.5 Hz, Ar-H), 7.67–7.89 (m, 5H, Ar-H), 9.75 (s, 1H, NH), 10.13 (s, 1H, NH), 11.25 (s, 1H, NH). ^{13}C NMR δ: 11.3, 14.2, 32.6, 41.2, 48.1, 61.3, 93.1, 111.3, 112.6, 128.8, 128.9, 129.7, 131.9, 134.2, 136.3, 137.3, 149.1, 154.1, 163.9, 166.7, 173.1. MS m/z (%): 460 (0.46, M^+), 77 (100.00). Anal. Calcd for $C_{26}H_{29}N_5O_3$ (459.55).

*5.1.5.4. Ethyl 6-(2-(4-chlorophenyl)-2-oxoethylamino)-4-(4-(dimethylamino) phenyl)-3-methyl-4,7-dihydro-1H-pyrazolo[3,4-b]pyridine-5-carboxylate **(9b)***. Yield 69%, m.p. 257–259 °C. IR: 3367, 3245, 3196 (3NH), 1715 (COOC$_2$H$_5$), 1688 (C=O). ^{1}H NMR δ: 1.29 (t, 3H, J = 7.5 Hz, OCH$_2$CH$_3$), 1.93 (s, 3H, CH$_3$), 2.98 (s, 6H, N(CH$_3$)$_2$), 4.24–4.29 (q, 2H, J = 7.5 Hz, OCH$_2$CH$_3$), 4.65 (s, 2H, CH$_2$), 4.96 (s, 1H, C$_4$-H), 6.68 (d, 2H, J = 7.0 Hz, Ar-H), 7.26 (d, 2H, J = 7.5 Hz, Ar-H), 7.61 (d, 2H, J = 7.5 Hz, Ar-H), 7.91 (d, 2H, J = 7.5 Hz, Ar-H), 9.76 (s, 1H, NH), 10.25 (s, 1H, NH), 11.21 (s, 1H, NH). ^{13}C NMR δ: 11.2, 14.2, 25.6, 30.4, 42.1, 48.8, 61.8, 90.0, 110.6, 117.3, 125.8, 128.2, 129.9, 130.6, 131.9, 136.3, 144.2, 154.4, 162.2, 165.7, 172.1. MS m/z (%): 496 (0.16, M^+ + 2), 494 (0.5, M^+), 135 (100.00). Anal. Calcd for $C_{26}H_{28}ClN_5O_3$ (493.99).

*5.1.5.5. Ethyl 6-(2-(4-bromophenyl)-2-oxoethylamino)-4-(4-(dimethylamino) phenyl)-3-methyl-4,7-dihydro-1H-pyrazolo[3,4-b]pyridine-5-carboxylate **(9c)***. Yield 66%, m.p. 247–248 °C. IR: 3378, 3256 (3NH), 1721 (COOC$_2$H$_5$), 1685 (C=O). ^{1}H NMR δ: 1.28 (t, 3H, J = 7.0 Hz, OCH$_2$CH$_3$), 1.84 (s, 3H, CH$_3$), 3.07 (s, 6H, N(CH$_3$)$_2$), 4.25–4.29 (q, 2H, J = 7.0 Hz, OCH$_2$CH$_3$), 4.51 (s, 2H, CH$_2$), 4.91 (s, 1H, C$_4$-H), 6.65 (d, 2H, J = 7.5 Hz, Ar-H), 7.23 (d, 2H, J = 7.5 Hz, Ar-H), 7.66 (d, 2H, J = 7.5 Hz, Ar-H), 7.98 (d, 2H, J = 7.5 Hz, Ar-H), 9.53 (s, 1H, NH), 9.78 (s, 1H, NH), 11.13 (s, 1H,

NH). ^{13}C NMR δ: 12.7, 13.9, 33.9, 41.9, 47.5, 61.8, 90.2, 110.4, 117.7, 127.8, 129.4, 130.3, 130.5, 131.6, 131.7, 136.1, 148.7, 152.6, 162.3, 169.7, 174.8. MS *m/z* (%): 540 (0.05, $M^+ + 2$), 538 (0.06, M^+), 77 (100.00). Anal. Calcd for $C_{26}H_{28}BrN_5O_3$ (538.44).

5.2. Biological evaluation

5.2.1. Antimicrobial and antiquorum-sensing evaluation

5.2.1.1. Antibacterial assay. Stock solutions (4000 μg/mL) of compounds **2–9** were prepared through their dissolution in DMSO. Two fold serial dilutions of test samples were done in LB (Luria-Bertani) broth, and various concentrations (2000, 1000, 500, 250, 125, 62.5, 31.25 and 15.625 μg/mL) were provided. Overnight cultures of *E. coli*, *P. aeruginosa*, *S. aureus* and *B. cereus* were diluted to 1×10^6 CFU/mL in LB broth. The diluted cultures (20 μL) were added to the test samples of different concentrations (50 μL) in 96-multiwell plates (all tests were performed once), then plates were incubated at 37 °C for 24 h [44–46]. The least concentrations of compounds prohibiting growth of bacteria (MICs) were detected visually (no turbidity), and compared to ampicillin.

5.2.1.2. Antifungal assay. Stock solutions (4000 μg/mL) of compounds **2–9** were prepared through their dissolution in DMSO. Two fold serial dilutions of test samples were done in glucose minimal medium, and various concentrations (2000, 1000, 500, 250, 125, 62.5, 31.25 and 15.625 μg/mL) were provided. *A. fumigatus* and *A. flavus* were diluted to 1×10^3 SFU/mL in glucose minimal medium, and *C. albicans* was diluted to 1×10^6 CFU/mL in Sabouraud's medium. The cultures (20 μL) were added to the test samples of different concentrations (50 μL) in 96-multiwell plates (all tests were performed once). For *A. fumigatus* and *A. flavus*, plates were incubated at 30 °C for 48 h, whereas for *C. albicans,* they were incubated at 37 °C for 48 h [44,45,47,48]. The least concentrations of compounds prohibiting growth of fungi (MICs) were detected visually (no turbidity), and compared to fluconazole.

5.2.1.3. Antiquorum-sensing assay. *C. violaceum* was grown in LB broth and incubated in an orbital incubator (150 rpm) at 30 °C for 16–18 h. The culture was adjusted to 0.5 McFarland standard (Ca. 1×10^6 CFU/mL). *C. violaceum* (50 μL) was inoculated into LB agar (50 mL), poured into plates and allowed to solidify. Wells were made in LB agar. Compounds **2–9** were dissolved in DMSO (5 mg/mL), and test samples (50 μL) were placed into the wells. Further, indole (positive control) was applied at the same concentration and volume to the plates. Additionally, DMSO (negative control) was applied to the plates. Plates were incubated at 30 °C for 48 h to examine the inhibition of violacein release. Bacterial growth inhibition results in a clear zone around the well, while QS inhibition is shown by a turbid zone harboring pigmentless bacterial cells of *C. violaceum* [44,45,49]. QS inhibition was calculated applying the equation $(r_2 - r_1)$ in mm; where r_2 is the total bacterial growth and pigment inhibition radius and r_1 is the bacterial growth inhibition radius.

5.2.2. Anticancer evaluation

5.2.2.1. In vitro anticancer assay using three cancer cell lines. HepG2, MCF-7 and Hela cancer cells were grown in Roswell Park Memorial Institute 1640 (RPMI-1640) medium supplied with 10% fetal bovine serum, penicillin (100 IU/mL) and streptomycin (100 μg/mL) under the atmosphere of 5% CO2 at 37 °C.

Cells were added to the 96-multiwell plates (10^4 cells/well) under the atmosphere of 5% CO_2 at 37 °C for 24 h to ensure that cells are attached to the wall of the plate. The solutions of compounds in DMSO were further diluted with phosphate buffer saline (PBS) to attain various concentrations. Compounds **2–9** of various concentrations were placed into the wells, and cells were kept with the compounds under the atmosphere of 5% CO_2 at 37 °C for 48 h (all tests were performed in triplicates). Cells were washed with PBS and 100 μL of 3-(4,5-dimethylthiazol-2-yl)-2,5-diphenyltetrazolium bromide solution (MTT) (5 mg/mL MTT stock in PBS diluted to 1 mg/mL with 10% RPMI-1640 medium) was added. The 96-multiwell plates were read by microarray reader Perkinelmer vector 3 V multilabel counter model 1420 (Perkinelmer, Boston, MA) for optical density at 490 nm [52–54]. The percentage cell viability was set as following:

$$\%\text{Cell viability} = \frac{A_{\text{treated cells}} - A_{\text{blank}}}{A_{\text{untreated cells}} - A_{\text{blank}}} \times 100$$

The relationship between % cell viability and compound concentration is plotted to attain the dose response curves for the three chosen cancer cells. Concentrations of compounds needed to inhibit 50% of cell viability (IC_{50}) were obtained from the curve fitting using Sigma plot10.

5.2.2.2. In vivo anticancer assay using EAC cells

5.2.2.2.1. Method. 8 Groups of mice ($n = 5$) were utilized, and the experiments were repeated three times [55–57].

Group 1: No EAC cells - received normal saline.
Group 2: EAC cells - received normal saline.
Group 3: EAC cells - treated intraperitoneally with **2** (100 mg/kg).
Group 4: EAC cells - treated intraperitoneally with **8a** (100 mg/kg).
Group 5: EAC cells - treated intraperitoneally with **8b** (100 mg/kg).
Group 6: EAC cells - treated intraperitoneally with **9b** (100 mg/kg).
Group 7: EAC cells - treated intraperitoneally with **9c** (100 mg/kg).
Group 8: EAC cells - treated intraperitoneally with DOX (100 mg/kg).

EAC cells (2×10^6) were inoculated intraperitoneally in each mouse (groups 2–8). After one day, compounds **2, 8a, 8b, 9b, 9c** and DOX were administered to mice for nine days, then blood samples were withdrawn for estimation of blood parameters.

5.2.2.2.2. Analysis of viable EAC cell count. Sample of EAC cells (100 μL, from three mice per group) was utilized and diluted twenty times with saline. Cells were stained with trypan blue, viable cells are not stained, while dead ones are stained. Viable cell count was determined.

5.2.2.2.3. Analysis of tumor volume. The ascetic fluid was gathered from the peritoneal cavity, and its volume was determined. It was then centrifuged and the packed tumor volume was measured.

5.2.2.3. In vitro cytotoxicity assay using two normal cell lines. Cytotoxic activity of pyrazolopyridines **2, 8a, 8b, 9b** and **9c** was tested according to the procedure described under *in vitro* anticancer testing [52–54].

5.2.3. DNA-binding assay

Methyl green/DNA (20 mg) was suspended in Tris-HCl buffer (0.05 M, 100 mL), pH 7.5, containing $MgSO_4$ (7.5 mM) and stirred at 37 °C for 24 h. Compounds **2, 3, 6, 7, 8a, 8b, 9b** and **9c** were dissolved in ethanol in eppendorf tubes, solvent was removed under vacuum and methyl green/DNA solution (200 μL) was placed into the tubes. The absorption maxima for methyl green/DNA complex is 642.5–645 nm. Samples were kept in dark at room temperature, and the absorbance of samples was set after 24 h [58]. Concentrations of compounds that cause initial absorbance of methyl green/DNA complex to be reduced by half (IC_{50}) were set.

5.3. Molecular modeling

2D Structures of the compounds were built and converted into 3D utilizing vLife MDS 3.0 software. 3D Structures were then energetically minimized up to the rms gradient of 0.01 utilizing the CHARMM22 force field. All conformers were then energetically minimized up to the rms gradient of 0.01. Molegro 2.5 [59] and Lead IT 2.3.2 [60] softwares were utilized for molecular docking studies, and LigandScout 4.1 software [61] was utilized to generate the pharmacophoric maps for compounds **2** and **9c**.

Acknowledgments

Gratitude to Holding Company for Biological Products and Vaccines (VACSERA), Egypt, for achieving anticancer and cytotoxicity testing.

Appendix A. Supplementary material

Supplementary data to this article can be found online at https://doi.org/10.1016/j.bioorg.2019.102976.

References

[1] B. Aslam, W. Wang, M.I. Arshad, M. Khurshid, S. Muzammil, M.H. Rasool, M.A. Nisar, R.F. Alvi, M.A. Aslam, M.U. Qamar, M.K.F. Salamat, Z. Baloch, Antibiotic resistance: a rundown of a global crisis, Infect. Drug Resist. 11 (2018) 1645–1658.

[2] J.O. Sekyere, J. Asante, Emerging mechanisms of antimicrobial resistance in bacteria and fungi: advances in the era of genomics, Future Microbiol. 13 (2018) 241–262.

[3] A. Kaur, N. Capalash, P. Sharma, Quorum sensing in thermophiles: prevalence of autoinducer-2 system, BMC Microbiol. 18 (62) (2018) 1–16, https://doi.org/10.1186/s12866-018-1204-x.

[4] D.S. Haque, F. Ahmad, S.A. Dar, A. Jawed, R.K. Mandal, M. Wahid, M. Lohani, S. Khan, V. Singh, N. Akhter, Developments in strategies for quorum sensing virulence factor inhibition to combat bacterial drug resistance, Microb. Pathog. 121 (2018) 293–302.

[5] G. Brackman, T. Coenye, Quorum sensing inhibitors as anti-biofilm agents, Curr. Pharm. Des. 21 (2015) 5–11.

[6] C.L. Chaffer, R.A. Weinberg, A perspective on cancer cell metastasis, Science 331 (2011) 1559–1564.

[7] W.A. Denny, DNA-intercalating ligands as anticancer drugs: prospects for future design, Anticancer Drug Des. 4 (1989) 241–263.

[8] M.F. Brana, M. Cacho, A. Gradillas, B. de Pascual-Teresa, A. Ramos, Intercalators as anticancer drugs, Curr. Pharm. Des. 7 (2001) 1745–1780.

[9] D. Agudelo, P. Bourassa, G. Bérubé, H.A. Tajmir-Riahi, Intercalation of antitumor drug doxorubicin and its analogue by DNA duplex: Structural features and biological implications, Int. J. Biol. Macromol. 66 (2014) 144–150.

[10] Z. Hajihassan, A. Rabbani-Chadegani, Studies on the binding affinity of anticancer drug mitoxantrone to chromatin, DNA and histone proteins, J. Biomed. Sci. 16 (31) (2009) 1–7, https://doi.org/10.1186/1423-0127-16-31.

[11] W.J. Sung, D.H. Kim, S.K. Sohn, J.G. Kim, J.H. Baek, S.B. Jeon, J.H. Moon, B.M. Ahn, K.B. Lee, Phase II trial of amsacrine plus intermediate-dose Ara-C (IDAC) with or without etoposide as salvage therapy for refractory or relapsed acute leukemia, Jpn. J. Clin Oncol. 35 (2005) 612–616.

[12] R. Martínez, L. Chacón-García, The search of DNA intercalators as antitumoral drugs: what it worked and what did not work, Curr. Med. Chem. 12 (2005) 127–151.

[13] R. Danesi, S. Fogli, A. Gennari, P. Conte, M. Del Tacca, Pharmacokinetic-pharmacodynamic relationships of the anthracycline anticancer drugs, Clin. Pharmacokinet. 41 (2002) 431–444.

[14] I.H. Eissa, A.M. El-Naggar, N.E.A. Abd El-Sattar, A.S.A. Youssef, Design and discovery of novel quinoxaline derivatives as dual DNA intercalators and topoisomerase II inhibitors, Anticancer agents Med. Chem. 18 (2018) 195–209.

[15] M.K. Ibrahim, M.S. Taghour, A.M. Metwaly, A. Belal, A.B.M. Mehany, M.A. Elhendawy, M.M. Radwan, A.M. Yassin, N.M. El-Deeb, E.E. Hafez, M.A. ElSohly, I.H. Eissa, Design, synthesis, molecular modeling and anti-proliferative evaluation of novel quinoxaline derivatives as potential DNA intercalators and topoisomerase II inhibitors, Eur. J. Med. Chem. 155 (2018) 117–134.

[16] I.H. Eissa, A.M. El-Naggar, M.A. El-Hashash, Design, synthesis, molecular modeling and biological evaluation of novel 1*H*-pyrazolo[3,4-*b*]pyridine derivatives as potential anticancer agents, Bioorg. Chem. 67 (2016) 43–56.

[17] K.J. Kripalani, J. Dreyfuss, J. Nemec, A.I. Cohen, F. Meeker, P. Egli, Biotransformation in the monkey of cartazolate (SQ 65,396), a substituted pyrazolopyridine having anxiolytic activity, Xenobiotica 11 (1981) 481–488.

[18] S.A. Thompson, P.B. Wingrove, L. Connelly, P.J. Whiting, K.A. Wafford, Tracazolate reveals a novel type of allosteric interaction with recombinant gamma-aminobutyric acid(A) receptors, Mol. Pharmacol. 61 (2002) 861–869.

[19] M. Marcade, J. Bourdin, N. Loiseau, H. Peillon, A. Rayer, D. Drouin, F. Schweighoffer, L. Désiré, Etazolate, a neuroprotective drug linking GABA(A) receptor pharmacology to amyloid precursor protein processing, J. Neurochem. 106 (2008) 392–404.

[20] H.S.H. Mohamed, M.N.M. Gad, A.M. El-zanaty, S.A. Ahmed, Synthesis, characterization and antibacterial activities of novel thieno, pyrazol pyridines and pyrazolopyrimidine derivatives, Der Pharma Chem. 10 (5) (2018) 121–127.

[21] T. Maqbool, A. Nazeer, M.N. Khan, M.C. Elliott, M.A. Khan, M. Ashraf, M. Nasrullah, S. Arshad, M.A. Munawar, Pyrazolopyridines II: Synthesis and antibacterial screening of 6-aryl-3-methyl-1-phenyl-1*H*-pyrazolo[3,4-*b*]pyridine-4-carboxylic acids, Asian J. Chem. 26 (2014) 2870–2872.

[22] W.S. Hamama, H.G. El-Gohary, M. Soliman, H.H. Zoorob, A versatile synthesis, PM3-semiempirical, antibacterial, and antitumor evaluation of some bioactive pyrazoles, J. Heterocycl. Chem. 49 (2012) 543–554.

[23] J. Quiroga, Y. Villarreal, J. Gálvez, A. Ortíz, B. Insuasty, R. Abonia, M. Raimondi, S. Zacchino, Synthesis and antifungal *in vitro* evaluation of pyrazolo[3,4-*b*]pyridines derivatives obtained by aza-Diels-Alder reaction and microwave irradiation, Chem. Pharm. Bull. 65 (2017) 143–150.

[24] N.S. El-Gohary, M.I. Shaaban, Design, synthesis, antimicrobial, antiquorum-sensing and antitumor evaluation of new series of pyrazolopyridine derivatives, Eur. J. Med. Chem. 157 (2018) 729–742.

[25] N.S. El-Gohary, M.I. Shaaban, New pyrazolopyridine analogs: Synthesis, antimicrobial, antiquorum-sensing and antitumor screening, Eur. J. Med. Chem. 152 (2018) 126–136.

[26] A. Hamza, H.A. El-Sayed, M.G. Assy, N.H. Ouf, M.E. Farhan, Synthesis and antimicrobial activity of some new triazine, 1,3-oxazine, fused pyridine and pyrimidine derivatives, World Appl. Sci. J. 36 (2018) 637–645.

[27] S.A. Abdel-Mohsen, T.I. El-Emary, New pyrazolo[3,4-*b*]pyridines: Synthesis and antimicrobial activity, Der Pharma Chem. 10 (4) (2018) 44–51.

[28] C. Samar, A. Ismail, T. Helmi, J. Khiari, J. Bassem, Substituted pyrazolo[3,4-*b*] pyridin-3-ones and pyrazolo[3,4-*b*]pyridine-5-carbaldehyde, new one-pot synthesis strategy amelioration using vinamidinium salts, antibacterial and antifungal activities promising environmental protection, J. Bacteriol. Parasitol. 8 (1000310) (2017) 1–8, https://doi.org/10.4172/2155-9597.1000310.

[29] M.S. Salem, M.A.M. Ali, Novel pyrazolo[3,4-*b*]pyridine derivatives: Synthesis, characterization, antimicrobial and antiproliferative profile, Biol. Pharm. Bull. 39 (2016) 473–483.

[30] J. Sindhu, H. Singh, J.M. Khurana, J.K. Bhardwaj, P. Saraf, C. Sharma, Synthesis and biological evaluation of some functionalized 1*H*–1,2,3-triazole tethered pyrazolo[3,4-*b*]pyridin-6(7*H*)-ones as antimicrobial and apoptosis inducing agents, Med. Chem. Res. 25 (2016) 1813–1830.

[31] H.N. Hafez, A.R.B.A. El-Gazzar, Synthesis of pyranopyrazolo *N*-glycoside and pyrazolopyranopyrimidine *C*-glycoside derivatives as promising antitumor and antimicrobial agents, Acta Pharm. 65 (2015) 215–233.

[32] P. Nagender, R.G. Malla, K.R. Naresh, Y. Poornachandra, K.C. Ganesh, B. Narsaiah, Synthesis, cytotoxicity, antimicrobial and anti-biofilm activities of novel pyrazolo [3,4-*b*]pyridine and pyrimidine functionalized 1,2,3-triazole derivatives, Bioorg. Med. Chem. Lett. 24 (2014) 2905–2908.

[33] M.A. El-Borai, H.F. Rizk, M.F. Abd-Aal, I.Y. El-Deeb, Synthesis of pyrazolo[3,4-*b*] pyridines under microwave irradiation in multi-component reactions and their antitumor and antimicrobial activities-Part 1, Eur. J. Med. Chem. 48 (2012) 92–96.

[34] M.A. El-Borai, H.F. Rizk, D.M. Beltagy, I.Y. El-Deeb, Microwave-assisted synthesis of some new pyrazolopyridines and their antioxidant, antitumor and antimicrobial activities, Eur. J. Med. Chem. 66 (2013) 415–422.

[35] M.A. El-Borai, M.K. Awad, H.F. Rizk, F.M. Atlam, Design, synthesis and docking study of novel imidazolyl pyrazolopyridine derivatives as antitumor agents targeting MCF7, Curr. Org. Synth. 15 (2018) 275–285.

[36] N.H. Metwally, E.A. Deeb, Synthesis, anticancer assessment on human breast, liver and colon carcinoma cell lines and molecular modeling study using novel pyrazolo [4,3-*c*]pyridine derivatives, Bioorg. Chem. 77 (2018) 203–214.

[37] H.S.P. Rao, L.N. Adigopula, K. Ramadas, One-pot synthesis of densely substituted pyrazolo[3,4-*b*]-4,7-dihydropyridines, ACS Comb. Sci. 19 (2017) 279–285.

[38] P. Nagender, R.N. Kumar, G.M. Reddy, D.K. Swaroop, Y. Poornachandra, C.G. Kumar, B. Narsaiah, Synthesis of novel hydrazone and azole functionalized pyrazolo[3,4-*b*]pyridine derivatives as promising anticancer agents, Bioorg. Med. Chem. Lett. 26 (2016) 4427–4432.

[39] B. Zhao, Y. Li, P. Xu, Y. Dai, C. Luo, Y. Sun, J. Ai, M. Geng, W. Duan, Discovery of substituted 1*H*-pyrazolo[3,4-*b*]pyridine derivatives as potent and selective FGFR kinase inhibitors, ACS Med. Chem. Lett. 7 (2016) 629–634.

[40] U. Fathy, A. Younis, H.M. Awad, Ultrasonic assisted synthesis, anticancer and antioxidant activity of some novel pyrazolo[3,4-*b*]pyridine derivatives, J. Chem. Pharm. Res. 7 (2015) 4–12.

[41] M.A.A. Elneairy, S.M. Eldine, A.S.I. Mohamed, Novel fused thienopyridine and pyrazolopyridine derivatives: Synthesis, characterization and cytotoxicity, Der Pharma Chem. 7 (5) (2015) 284–295.

[42] M.A. Tabrizi, P.G. Baraldi, S. Baraldi, F. Prencipe, D. Preti, G. Saponaro, R. Romagnoli, S. Gessi, S. Merighi, A. Stefanelli, D. Fazzi, P.A. Borea, R.C. Maia, N.C. Romeiro, C.A. Fraga, E.J. Barreiro, Synthesis and biological evaluation of pyrazolo[3,4-*b*]pyridin-4-ones as a new class of topoisomerase II inhibitors, Med. Chem. 11 (2015) 342–353.

[43] N.R. Mohamed, N.Y. Khaireldin, A.F. Fahmy, A.A. El-Sayed, Facile synthesis of fused nitrogen containing heterocycles as anticancer agents, Der Pharma Chem. 2 (1) (2010) 400–417.

[44] N.S. El-Gohary, M.I. Shaaban, Synthesis, antimicrobial, antiquorum-sensing, and cytotoxic activities of new series of isoindoline-1,3-dione, pyrazolo[5,1-*a*]isoindole and pyridine derivatives, Arch. Pharm. Chem. Life Sci. 348 (2015) 666–680.

[45] N.S. El-Gohary, M.I. Shaaban, Antimicrobial and antiquorum-sensing studies. Part 3: Synthesis and biological evaluation of new series of [1,3,4]thiadiazole and fused [1,3,4]thiadiazole derivatives, Arch. Pharm. Chem. Life Sci. 348 (2015) 283–297.

[46] Clinical Laboratory Standards Institute (CLSI), Performance Standards for Antimicrobial Susceptibility Testing; Twenty-Fifth Informational Supplement. Clinical and Laboratory Standards Institute, Wayne, PA, USA (2015) M100-S25.

[47] Clinical Laboratory Standards Institute (CLSI), Reference Method for Broth Dilution Antifungal Susceptibility Testing of Yeasts; Approved Standard-Third Edition. Clinical and Laboratory Standards Institute, Wayne, PA, USA (2008) M27-A3.

[48] Clinical Laboratory Standards Institute (CLSI), Reference Method for Broth Dilution Antifungal Susceptibility Testing of Filamentous Fungi; Approved Standard-Second Edition. Clinical and Laboratory Standards Institute, Wayne, PA, USA (2008) M38-A2.

[49] K.H. McClean, M.K. Winson, L. Fish, A. Taylor, S.R. Chhabra, M. Camara, M. Daykin, J.H. Lamb, S. Swift, B.W. Bycroft, G.S. Stewart, P. Williams, Quorum

sensing and *Chromobacterium violaceum*: exploitation of violacein production and inhibition for the detection of *N*-acyl homoserine lactones, Microbiology 143 (1997) 3703–3711.
[50] R. McClean, L.S. Pierson, C. Fuqua, A simple screening protocol for the identification of quorum signal antagonists, J. Microbiol. Methods 58 (2004) 351–360.
[51] W. Cha, D.A. Vattem, V. Maitin, M.B. Barnes, R.J. Mclean, Bioassays of quorum sensing compounds using *Agrobacterium tumefaciens* and *Chromobacterium violaceum*, Methods Mol. Biol. 692 (2011) 3–19.
[52] T. Mosmann, Rapid colorimetric assay for cellular growth and survival: Application to proliferation and cytotoxicity assays, J. Immunol. Methods 65 (1983) 55–63.
[53] F. Denizot, R. Lang, Rapid colorimetric assay for cell growth and survival. Modifications to the tetrazolium dye procedure giving improved sensitivity and reliability, J. Immunol. Methods 89 (1986) 271–277.
[54] D. Gerlier, T. Thomasset, Use of MTT colorimetric assay to measure cell activation, J. Immunol. Methods 94 (1986) 57–63.
[55] C. Oberling, M. Guerin, The role of viruses in the production of cancer, Adv. Cancer Res. 2 (1954) 353–423.
[56] K.R. Sheeja, G. Kuttan, R. Kuttan, Cytotoxic and antitumour activity of Berberine, Amala Res. Bull. 17 (1997) 73–76.
[57] B.D. Clarkson, J.H. Burchenal, Preliminary screening of antineoplastic drugs, Prog. Clin. Cancer 1 (1965) 625–629.
[58] N.S. Burres, A. Frigo, R.R. Rasmussen, J.B. McAlpine, A colorimetric microassay for the detection of agents that interact with DNA, J. Nat. Prod. 55 (1992) 1582–1587.
[59] R. Thomsen, M.H. Christensen, MolDock: a new technique for high accuracy molecular docking, J. Med. Chem. 49 (2006) 3315–3321.
[60] LeadIT version 2.3.2; BioSolveIT GmbH, Sankt Augustin, Germany, 2017, www.biosolveit.de/LeadIT.
[61] G. Wolber, T. Langer, LigandScout: 3D Pharmacophores derived from protein bound ligands and their use as virtual screening filters, J. Chem. Inf. Comput. Sci. 45 (2005) 160–169.
[62] R.U. Kadam, N. Roy, Recent trends in drug likeness prediction: a comprehensive review of *in silico* methods, Ind. J. Pharm. Sci. 69 (2007) 609–615.
[63] C.A. Lipinski, F. Lombardo, B.W. Dominy, P.J. Feeney, Experimental and computational approaches to estimate solubility and permeability in drug discovery and development settings, Adv. Drug Deliv. Rev. 46 (2001) 3–26.
[64] http://www.molinspiration.com/cgi-bin/properties.
[65] D.F. Veber, S.R. Johnson, H.Y. Cheng, B.R. Smith, K.W. Ward, K.D. Kopple, Molecular properties that influence the oral bioavailability of drug candidates, J. Med. Chem. 45 (2002) 2615–2623.
[66] https://preadmet.bmdrc.kr/toxicity/.
[67] http://molsoft.com/mprop/.